ASEN 6061 Project 1: Test Particle Monte Carlo

Kalvin Y. Monroe∗
University of Colorado, Boulder, CO, 80303

The effect of nonequilibrium wall temperatures on rarefied gas flow is investigated. A test particle Monte Carlo code (TPMC) was developed to explore this. In this paper, (TPMC) methodology and results are presented for the flow of Nitrogen (N_2) at 300 K from an equilibrium reservoir through a cylindrical tube. Multiple wall temperatures are considered, ranging from 1 to 10 times the reservoir temperature. Finally, gas and surface properties along the cylinder axis are calculated. Properties include number density, temperature, pressure, heat transfer, and shear stress. Results show evolution of properties over time due to the nonequilibrium wall.

I. Nomenclature

TPMC	=	Test particle monte carlo
Kn	=	Knudsen number
T_w	=	Wall temperature [K]
T	=	Reservoir temperature [K]
d	=	Cylinder diameter [m]
r	=	Cylinder radius [m]
a	=	Thermal accommodation coefficient
L	=	Cylinder length [m]
n	=	Number density [m^{-3}]
N	=	Number of simulated particles
P	=	Pressure [Pa]
σ	=	Axial shear stress [Pa]
q	=	Heat transfer [W/m^2]
$\bar{\mathbf{u}}$	=	Bulk velocity [m/s]
$\bar{\mathbf{u}}'$	=	Thermodynamic fluctuating velocity[m/s]
m	=	mass of N_2 [kg]
k_b	=	Boltzmann constant [J/K]
$\mathbf{e_x}$	=	Cartesian x-direction unit vector
$\mathbf{e_y}$	=	Cartesian y-direction unit vector
$\mathbf{e_z}$	=	Cartesian z-direction unit vector
$\mathbf{e_x^*}$	=	Wall-normal x-direction unit vector
$\mathbf{e_y^*}$	=	Wall-normal y-direction unit vector
$\mathbf{e_z^*}$	=	Wall-normal z-direction unit vector
$\mathbf{u}$	=	Cartesian velocity vector
$\mathbf{u}^*$	=	Wall-normal velocity vector

II. Introduction

The applications of rarefied gas flows have long been studied over a range of topics, including re-entry vehicles and orbital dynamics. A gas can be considered to be rarefied if it's Knudsen number, defined as the ratio of the molecular mean free path λ to a characteristic length L, is $O(10^{-1})$ or larger.

$$Kn = \frac{\lambda}{L} \tag{1}$$

∗PhD Student, Ann and H.J. Smead Aerospace Engineering Sciences

When $Kn << 1$, continuum dynamics governed by the Navier-Stokes equations can be assumed. A continuum suggests that local thermodynamic fluctuations are small compared to flow gradients, and thus, local thermodynamic equilibrium us assumed. Continue dynamics also assume the no-slip condition, where the fluid velocity goes to zero at a solid wall. These assumptions, however, break down for rarefied flows. In this regime, particle collisions and energy exchanges are not frequent, resulting in non-negligible gradients in thermodynamic properties. Additionally, due to large intermolecular spacing, the no-slip condition is no longer true. At extremely high Knudsen numbers $Kn >> 1$, the free-molecular limit is reached, where particle-particle collisions are ignored entirely, and only particle interaction with boundaries is considered.

In the free-molecular limit, as particle-particle collisions are ignored, particles can be simulated and tracked one at a time. Mean properties through the domain can then be calculated as a sum of contributions from each particle. This is the underlying basis of the Test Particle Monte Carlo Code (TPMC). In this study, TPMC is used to study effusion of a gas at equilibrium through a cylinder at varying wall temperatures. Observations of the non-equilibrium region within the cylinder are observed as particles interact with the boundaries.

First the methodology behind the TPMC code is explained in detail. Next, validation of the TPMC code is presented. Finally, results of the TPMC code against varied wall temperatures, thermal accommodation coefficients, and cylinder lengths are discussed.

III. TPMC Methodology

A. Simulation Setup

The test problem to apply the TPMC code is the effusion of diatomic Nitrogen through a cylindrical tube of diameter d. Its length L is variable and chosen to be either 1, 5, 10, or 20 mm. Particles from the equilibrium reservoir enter the cylinder through the inlet and either exit the cylinder out the vacuum outlet, or the inlet. Particles have varied bulk velocities in the x-direction, $\bar{\mathbf{u}} \in [0, 422, 1000, 7800]$ m/s. The reservoir is defined to have a temperature of $T = 300$ K. N_2 has a diameter of 4.65×10^{-10} and a mass of $m = 4.65 \times 10^{-26}$. Fig. 1 shows a drawing of the simulated problem. Note that the cartesian basis is defined such that the x-direction is aligned with the axis of the cylinder. Wall-normal coordinates are defined such that the x-direction is coincident with it's cartesian analog, with y- and z- directions being normal and tangent to the cylinder surface, respectively.

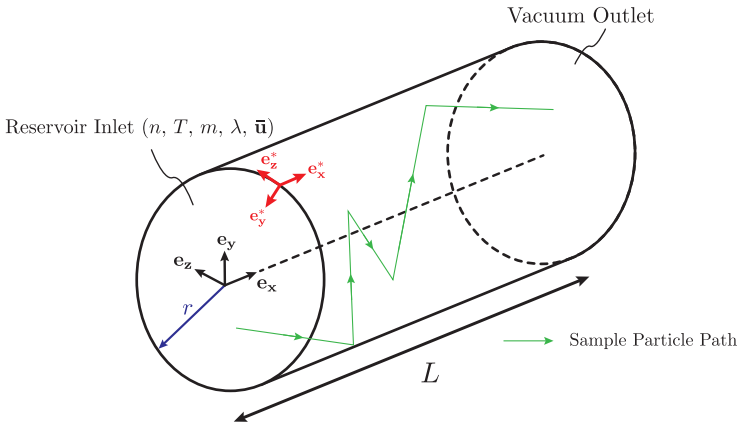

Fig. 1 TPMC cylinder geometry with equilibrium inlet and vacuum outlet.

Within the equilibrium reservoir, the velocity each particle direction adheres to a single component Maxwell-Boltzmann distribution of the form in Eq. 2.

$$f(u') = \left(\frac{m}{2\pi kT}\right)^{1/2} e^{-\frac{m}{2kT}(u')^2} \tag{2}$$

When entering the cylinder, particle velocity components in the y- and z-directions can be sampled from this distribution using an inverse cumulative method as described in Bird [1]. However, with regard to the x-direction, special attention must be made in sampling its velocity. Specifically, we expect that the velocity in the x-direction to be

positive for incoming particles. To get this behavior, we sample from a biased Maxwell-Boltzmann distribution using an acceptace-rejection method, described in Boyd and Schwartzentruber [2]. This results in the expression shown in Eq. 3 for the particle number flux in particles / unit time / unit area through the inlet

$$\dot{N}_i = \frac{1}{4} n_i \sqrt{\frac{8kT}{\pi m}} \left[exp(-s_1^2) + \sqrt{\pi} s_1 (1 + erf(s_1)) \right] \tag{3}$$

where $s_1 = \bar{u}_1 / C_{mp}$ is the ratio of the bulk velocity in the x-direction to the most probable speed, defined as $C_{mp} = \sqrt{2kT/m}$. For the TPMC code, the number of simulated particles is chosen by the user and the area of the cylinder is a simulation parameter. This means that the total timestep can be calculated in Eq. 4 as

$$dt = \frac{N}{\dot{N}_i \pi r^2} \tag{4}$$

B. Particle-Wall Collision

When a particle hits the wall, its velocity post collision is governed by the thermal accommodation coefficient, $a \in [0, 1]$. For a value of $a = 0$, each collision with the wall will be *specular*, where the velocity in the $\mathbf{e}_\mathbf{y}^*$ direction is simply reversed. For $a = 1$, each collision with the wall will be *diffuse*. For diffuse collisions, velocities in the $\mathbf{e}_\mathbf{x}^*$ and $\mathbf{e}_\mathbf{z}^*$ directions are sampled from a Maxwell-Boltzmann distribution (Eq. 2) using the wall temperature. Akin to the treatment at the inlet, velocity in the $\mathbf{e}_\mathbf{y}^*$ direction is sampled from a biased Maxwell-Boltzmann distribution using the wall temperature - ensuring that the wall normal velocity post collision is positive. It is important to note, however, that the bulk velocity of any particle after a collision with the wall is set to 0 for a diffuse collision, but remains the same for a specular collision. For values of $0 < a < 1$, for each collision a random number $r_n \in [0, 1]$ is generated. If $r_n > a$, then the collision is diffuse, while for $r_n < a$ collisions are specular.

To calculate properties in the wall-normal coordinate system, we first note that the wall-normal unit vectors can be calculated from a cartesian basis by

$$\mathbf{e}_\mathbf{x}^* = [1, 0, 0] \tag{5}$$

$$\mathbf{e}_\mathbf{y}^* = \frac{[0, -y, -z]}{\sqrt{y^2 + z^2}} \tag{6}$$

$$\mathbf{e}_\mathbf{z}^* = \frac{\mathbf{e}_\mathbf{x} \times \mathbf{e}_\mathbf{y}}{|\mathbf{e}_\mathbf{x} \times \mathbf{e}_\mathbf{y}|} \tag{7}$$

Using these unit vectors, we can define a coordinate transformation matrix $A = [\mathbf{e}_\mathbf{x}^*, \mathbf{e}_\mathbf{y}^*, \mathbf{e}_\mathbf{z}^*]$, comprised of the three wall-normal unit vectors as column entries. From this, a transformation of a velocity vector $\mathbf{u}$ from cartesian to wall-normal coordinates, or vice versa, is a simple matrix operation, as seen in Eqs. 8 and 9.

$$\mathbf{u} = \mathbf{A}\mathbf{u}^* \tag{8}$$

$$\mathbf{u}^* = \mathbf{A}^{-1}\mathbf{u} \tag{9}$$

Given a particle initial location $[x_0, y_0, z_0]$ and velocity $\mathbf{u} = [u, v, w]$, the location of its eventual collision with the wall is paramount to understanding its path through the cylinder. Luckily, an analytical solution exits to find the collision location. By solving the quadratic equation in Eq. 10 for the time to a collision with the cylinder wall t, where the coefficients are given in Eqns. 11, 12, and 13. The smallest, real, positive root of the quadratic equation will be the time it takes for the particle to hit the wall.

$$At^2 + Bt + C = 0 \tag{10}$$

$$A = v^2 + z^2 \tag{11}$$

$$B = 2(y_0 v + z_0 w) \tag{12}$$

$$C = y_0^2 + z_0^2 - R^2 \tag{13}$$

There is also the case where the particle makes contact with the inlet or outlet. This is also an important boundary condition, as for a TPMC code, we remove the particle from the system when this occurs. Again, there are analytical solutions to determining at what time a particle will interact with an inlet/outlet. Knowing a point on the plane $\mathbf{p} = [p_x, p_y, p_z]$ and normal vector $\hat{\mathbf{n}} = [n_x, n_y, n_z]$, the time to the interaction is given by Eq. 14. Between Eqns. 10 and 14, the smallest positive time will be the first interaction with a boundary a particle will see.

$$t = \frac{n_x(p_x - x_0) + n_y(p_y - y_0) + n_z(p_z - z_0)}{n_x u + n_y v + n_z w} \tag{14}$$

C. TPMC Procedure

The general workflow of the TPMC code is described below.

1) User specifies equilibrium reservoir variables (T,m,λ,$\bar{\mathbf{u}}$)
2) A particle is created with an initial location randomly chosen on the inlet surface.
3) The particle velocity is sampled from a Maxwell-Boltzmann distribution for the y- and z- directions, and a biased distribution for the x-direction. This includes any bulk velocity associated with the reservoir.
4) Eqns. 10 and 14 are solved to obtain the time t until a particle interacts with either the cylinder wall or inlet.
5) Particle path is propagated from its initial location for the solved time t.
6) Over the path of the particle, update state bins for the gas properties of the cylinder (N, T)
    1) If a particle interacts with a domain inlet/outlet, then delete it.
    2) Otherwise, the particle hits a cylinder wall. Choose the reflection type (diffuse or specular) and update the particle velocity.
    3) Update state bins for surface properties (q, p, σ)
7) Loop back to step 4 until the particle exits the domain. Then restart at step 2 until all particles are generated, as determined in by the user.

This methodology was implemented in python. A particle class was created to store information about each particle in an organized manner. Equations for updating each state bin can be found in the Appendix VI.

IV. TPMC Validation

To validate this python code, values were compared to previous codes with known outputs. Specifically, a study by Davis [3] provides a test simulation to compare to. For a cylinder with radius $r = L$, fully diffuse collisions, and wall temperature equal to the reservoir temperature, it is expected that the fraction of particles exiting the outlet with no wall collisions is $N_d/N = 0.3820$, and with collisions to be $N_t/N = 0.6720$. Table 1 show a similar study using the created python code.

N	T_{inlet}	N_d/N	N_t/N
100	406.7	0.32	0.634
1000	403.2	0.36	0.679
10000	399.7	0.364	0.663
100000	400.0	0.367	0.658

Table 1 TPMC Validation Results

Seen above, the implementation of the TPMC code in python produces reasonable results compared to the study by Davis [3]. Expected fractions of particles leaving the outlet with and with collisions are in agreement to expected values by less than 2%. This suggests that the TPMC methodology was implemented correctly.

Additionally, from a visual perspective, specular and diffusive reflections will have certain behaviors that can indicate if particle reflections are properly implemented. As specular reflections only reverse the normal component of velocity, it is expected that each particle will have symmetric reflection from the wall, and will be guaranteed to travel to the outlet of the cylinder. Diffuse reflections, as velocity components are sampled, are expected to have more of a random visual behavior, and are not guaranteed to reach the end of the cylinder. Sample paths from a fully specular and fully

diffuse cases are shown below in Fig 2. It is observed that the expected behavior for each reflection type is recovered. This supports the conclusion that the TPMC code is properly implemented.

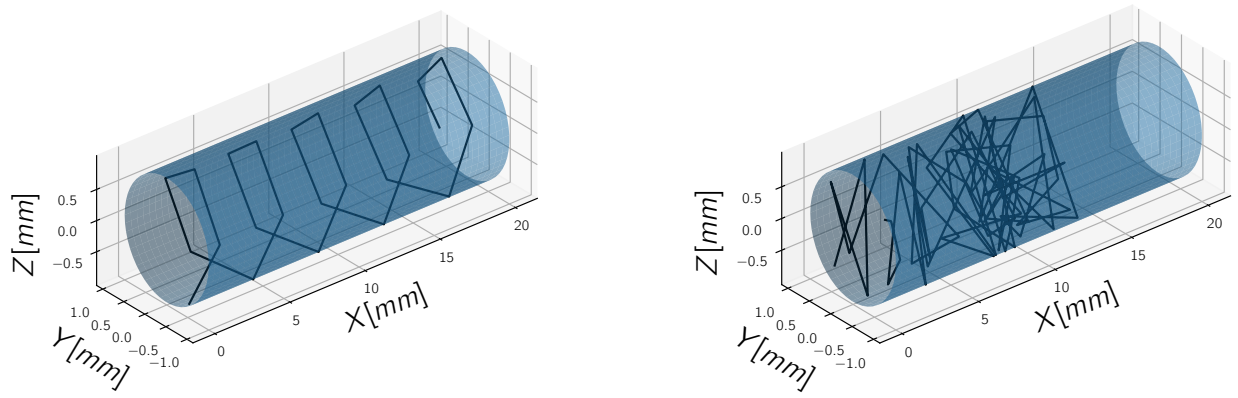

Fig. 2 Sample particle paths for specular (left) and diffuse (right) reflections.

In addition, a similar case was run to the one described above, with the only change being all reflections were set to be specular. As normal velocity is simply reversed at a wall collision, energy is conserved, and therefore we can expect certain behaviors on the pressure, heat transfer, number density, and shear stress along the cylinder. According to the formulations of each quantity seen in Appendix VI, we can expect pressure to be constant along the entire length. Additionally, we will observe heat transfer and shear stress to be nominally zero and the velocity magnitude of each particle stays constant, and thus, no energy is transferred to the wall. Adding on, as all particles will retain their initial positive x-velocity, we can expect the number density to be constant along the cylinder. Viewing Figs. 3, 4, 5, and 6, this behavior is recovered.

Finally, a verification test was performed on the particle velocity sampling procedures to ensure that sampled velocities followed either a Maxwell Botlzmann distribution, or a biased Maxwellian. This process occurs during the creation of a particle, as well as during a diffuse particle collision. Fig. 7 shows that the sampled velocities in the x-, y-, and z- directions for 100000 seem to conform to the expected results of each distribution.

V. Results and Discussion

The TPMC code has many user-tunable parameters. This creates a large parameter space that is intractable for the purposes of this report. For this reason the choice is made to restrict the parameter space. Wall temperature is varied from $T_w/T = 0.1, 1, 10$, and bulk x-velocity is varied from $\bar{u}_1 = 0, c_m', 1000, 7800$ m/s, where c_m' is the mean thermal velocity of the particles, equal to 422 m/s. The cylinder length is held constant at $L = 20$ mm. 10000 particles were simulated for each run. Following Eq. 4, this corresponds to a timestep of $\Delta t = 2.68 \times 10^{-12}$. Only fully diffuse collisions are simulated. Only plots of gas temperature, pressure, number density, and heat transfer are considered.

A. $T_w/T = 0.1$

Figs. 8, 9, 10, and 11 show plots of gas temperature, pressure, number density, and heat transfer respectively. Looking to temperature, we first observe that near the entrance of the cylinder, there is a sharp region where particles are equilibrating with the wall temperature and increase in temperature - approaching $\frac{4}{3}T \times \frac{T}{T_w} = 40$ K. This corresponds well to the peak in heat transfer, where energy is seen to be transferred to the particles. Number density is observed to decrease along the cylinder. This can be explained as since diffuse particles have no preferential direction it is possible for them to return towards the inlet. As the bulk velocity increases, a local maximum in the pressure tends to form near the center of the cylinder. This is in agreement with the peak in number density, where we expect collisions to be highest. The heat transfer for the $\bar{u}_1 = 7800$ m/s case is extremely noisy as the high bulk velocity does not make it probable for as many particles to hit the cylinder walls compared to the slower cases. This also can explain the failure of this case to reach temperature equilibrium with the wall.

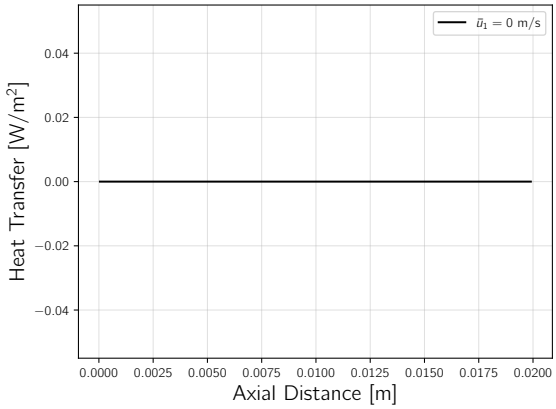

Fig. 3 Heat transfer in a fully specular case for $T_w/T = 1$

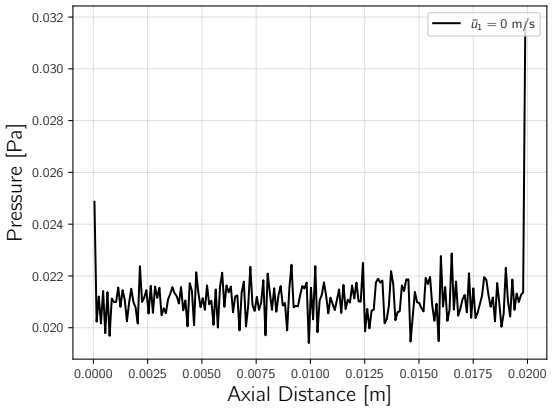

Fig. 4 Pressure in a fully specular case for $T_w/T = 1$

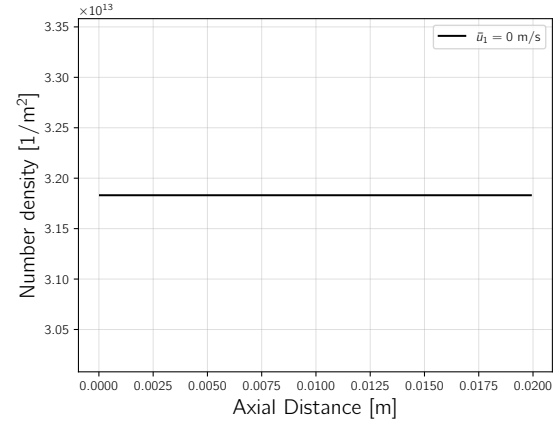

Fig. 5 Number density in a fully specular case for $T_w/T = 1$

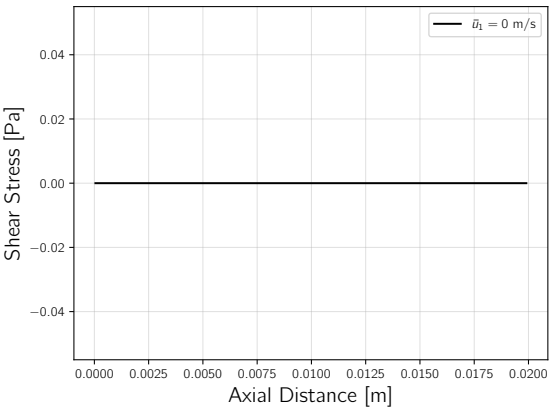

Fig. 6 Shear stress in a fully specular case for $T_w/T = 1$

B. $T_w/T = 1$

Figs. 12, 13, 14, and 15 show plots of gas temperature, pressure, number density, and heat transfer respectively. Looking to temperature, we first observe that for the zero bulk velocity case the average velocity is near 400 K. This is expected, as discussed in section IV. As inlet bulk velocity is increased, we see that the average inlet temperature decreases towards the temperature of the equilibrium reservoir. Again this is expected as with a bulk velocity in the x-direction, the original Maxwell-Boltzmann of the equilibrium particles in the x-direction is shifted to the right, and therefore, the average thermal energy of the biased maxwellian is expected to be closer to the thermal average of the reservoir. We also note that as particles collide with the wall, temperature tends to the expected temperature of $\frac{4}{3}T \times \frac{T}{T_w} = 400$ K. However, near the exit, temperature is seen to decrease again. The reasoning for this behavior is unknown and should be investigated in the future. Looking at pressure, we see that as inlet bulk velocity is increased, a local maximum in the pressure is observed near the middle of the cylinder. This is in agreement with the peak in number density, where we expect collisions to be highest. In regard to heat transfer, it is observed that the peak in heat transfer occurs near the entrance of the cylinder at $x = 2.5$ mm. The heat transfer for the $\bar{u}_1 = 7800$ m/s case is extremely noisy as the high bulk velocity does not make it probably for as many particles to hit the cylinder walls compared to the slower cases.

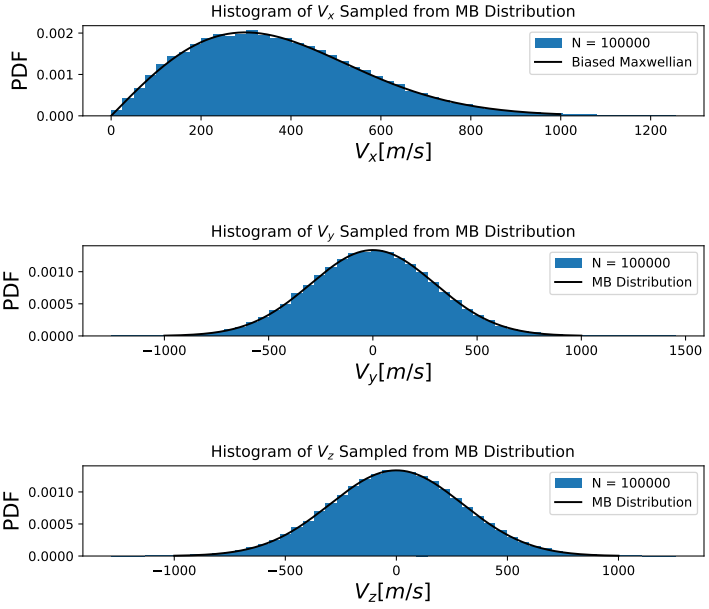

Fig. 7 Particle velocity sampling distributions follow expected results.

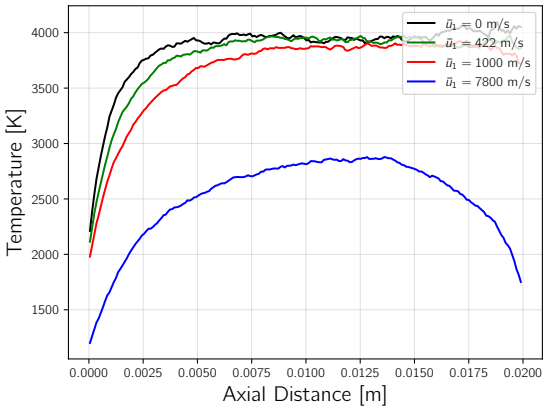

Fig. 8 Axial temperature distribution for $T_w/T = 0.1$

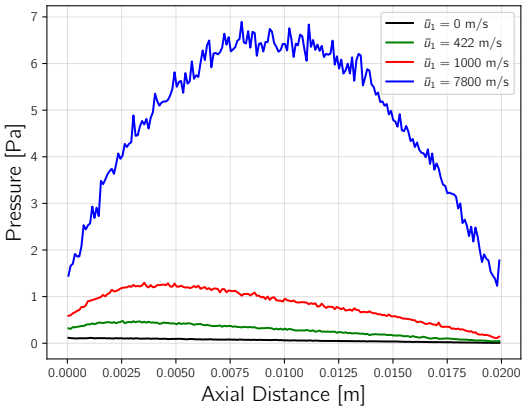

Fig. 9 Axial pressure distribution for $T_w/T = 0.1$

C. $T_w/T = 10$

Figs. 16, 17, 18, and 19 show plots of gas temperature, pressure, number density, and heat transfer respectively. Looking to temperature, we first observe that near the entrance of the cylinder, there is a sharp region where particles are equilibrating with the wall temperature and increase in temperature - approaching $\frac{4}{3}T \times \frac{T}{T_w} = 4000$ K. This corresponds well to the peak in number density and heat transfer, where energy is seen to be transferred to the particles. However, an increase in temperature is agian observed near the exit. This behavior is unexplained at the moment, as it would be unexpected for particles at equilibrium with the wall to increase in temperature. As the bulk velocity increases, a local maximum in the pressure tends to form near the center of the cylinder. The heat transfer for the $\bar{u}_1 = 7800$ m/s case is extremely noisy as the high bulk velocity does not make it probably for as many particles to hit the cylinder walls compared to the slower cases. This also can explain the failure of this case to reach temperature equilibrium with the wall.

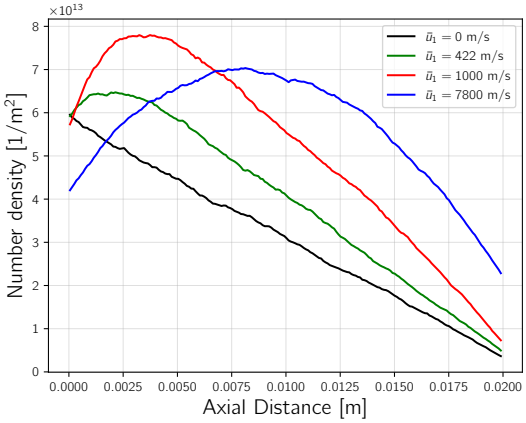

Fig. 10 Number density distribution for $T_w/T = 0.1$

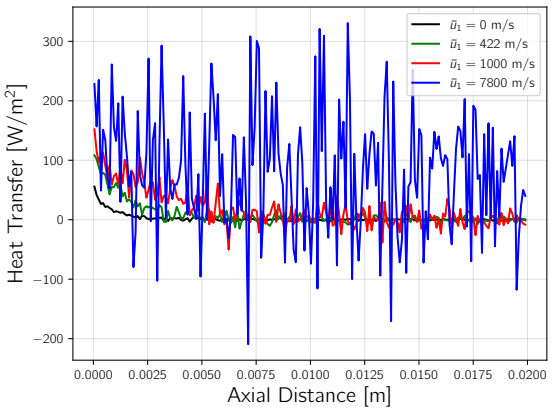

Fig. 11 Heat transfer distribution for $T_w/T = 0.1$

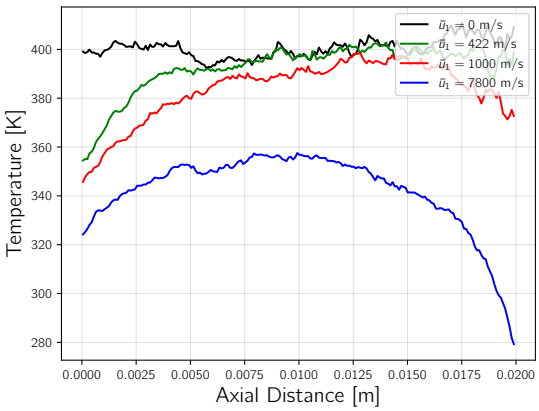

Fig. 12 Axial temperature distribution for $T_w/T = 1$

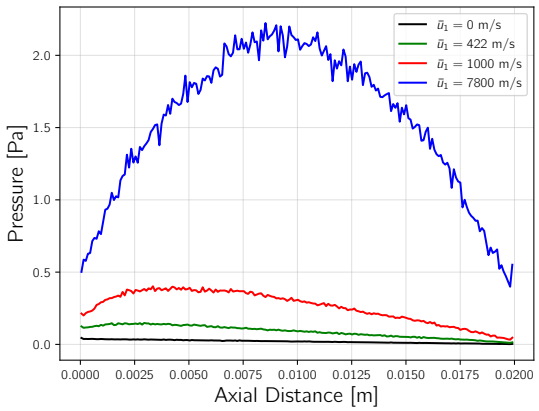

Fig. 13 Axial pressure distribution for $T_w/T = 1$

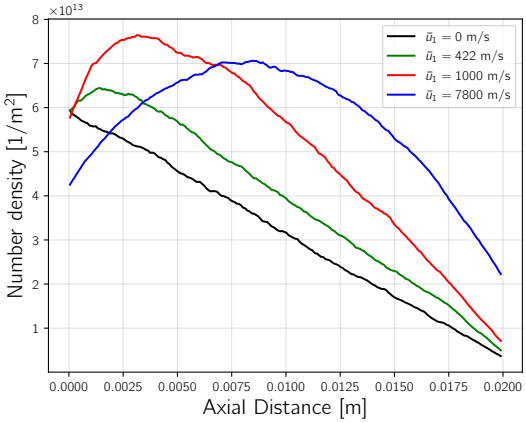

Fig. 14 Number density distribution for $T_w/T = 1$

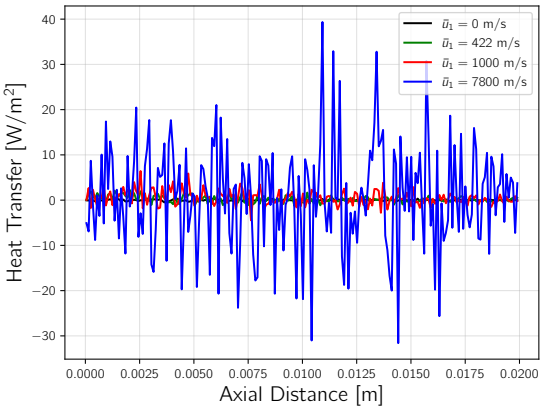

Fig. 15 Heat transfer distribution for $T_w/T = 1$

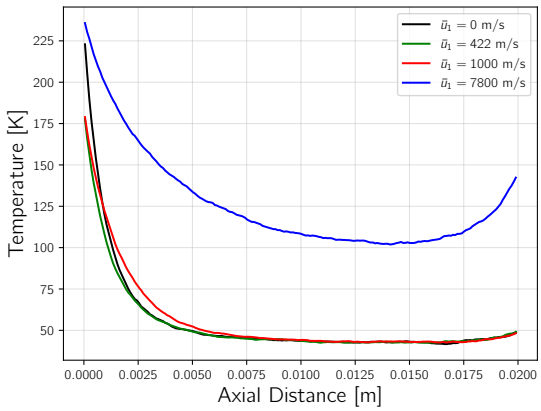

Fig. 16 Axial temperature distribution for $T_w/T = 10$

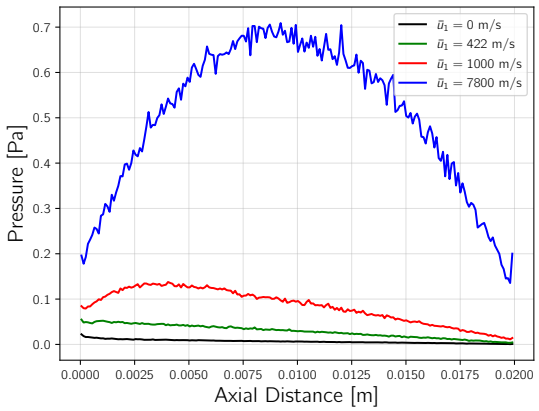

Fig. 17 Axial pressure distribution for $T_w/T = 10$

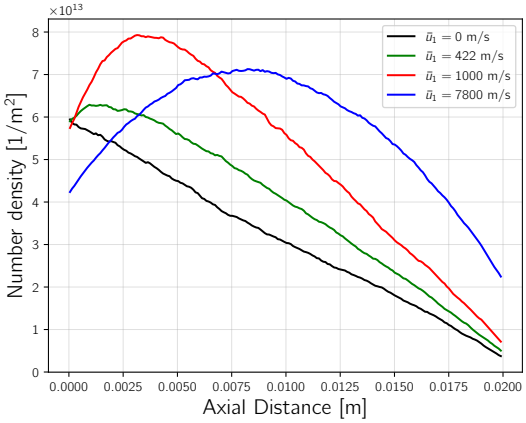

Fig. 18 Number density distribution for $T_w/T = 10$

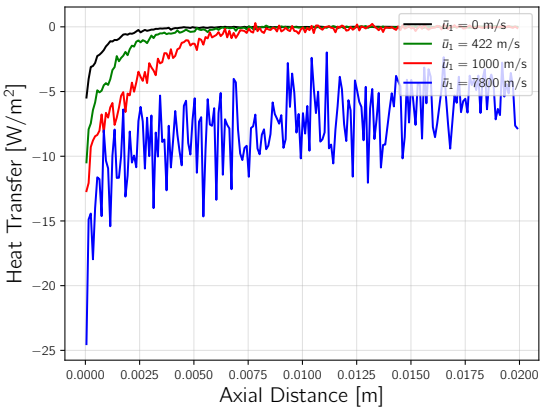

Fig. 19 Heat transfer distribution for $T_w/T = 10$

VI. Conclusion

A TPMC code was created in python for the purposes of simulating effusion through a cylindrical opening. The code has the ability to vary the wall temperature, bulk inflow velocity, reservoir conditions, thermal accommodation coefficient, cylinder length, and number of simulated particles. The TPMC code was validated against a previous study, and its methodology was explained in detail. For three different wall temperatures, plots of gas temperature, pressure, number density, and heat transfer were created with plots for four separate bulk velocities.

For all cases, it was observed that interactions with the wall serve to push the system to equilibrium. This is best observed in the plots of temperature and heat transfer, where temperature approaches the wall temperature, and heat transfer tends to go to 0. However, for the case of $\bar{u}_1 = 7800$ m/s, many times the system does not reach equilibrium. This is due to the fact that the inflow is so fast that there is not enough time for enough collisions to occur within the cylinder for the system to equilibrate. Also, due to this behavior data from this case was considerably noisy. Future work would suggest the use of more simulated particles, perhaps $N = 1000000$, such that the noise level of this case can be reduced. Number densities were observed to decrease along the length of the cylinder due to the chance of diffuse reflection to result in particles traveling back upstream. Peaks in pressure were observed to occur in the same general locations as number density and temperature. This is understandable as the high temperature particles will be faster and can impart more momentum to the surface as pressure. Other suggested work would be to investigate odd inlet/outlet behaviors. Specifically these include the observations of changing temperature near the outlet, seen in Figs. 16, 12, and 8 and spikes in pressure, seen in Fig. 4.

Appendix A

Within the TPMC code, the domain in the x-direction was split into $n_x = 200$ cells, symmetric in the y- and z-directions. The size of each cell was therefore calculated as $\Delta x = n_x/L$. Gas properties were calculated at each cell, using a cell-centered discretization. Surface properties were binned into each cell surface element of $\Delta A = \Delta x \pi (d/2)^2$. The cell volume could be calculated as $\Delta V = \Delta A \pi d$.

For cell volume properties, we denote p as a particle that crosses a cell j. Number density of a cell n^j is calculated simply as the total number of particles that cross the cell divided by the cell volume, seen below as

$$n_j = \frac{\sum p}{\Delta V} \tag{15}$$

We also denote $< u_i' >= u_i - < u_i >$ as the thermal component of a velocity in the i direction of a particle p, where $< u_i >$ is the expected velocity component in the same direction. The temperature contribution of this particle towards a cell can be calculated as shown in Eq. 20. Summing this relation for every particle contribution results in the final temperature of the cell.

$$T_j = \frac{m}{3k_b}(< u_1'^2 > + < u_2'^2 > + < u_3'^2 >) \tag{16}$$

For cell surface quantities, we define p_{col} as a particle that hits the wall of a cell. Similar to Eq. 15, the collision frequency is found through Eq. 17, where Δt is found using Eq. 4.

$$Col_j = \frac{\sum p}{\Delta A \Delta t} \tag{17}$$

Pressure P and axial shear stress σ are calculated using the difference in normal velocity and axial velocity respectively after a collision with the wall. We denote the velocities before and after a collision in wall coordinates as $\mathbf{u}^*_{pre}$ and $\mathbf{u}^*_{post}$. The contribution to pressure and shear stress by each particle can be found using Eq. 18 and 19.

$$P_j = \frac{m}{\Delta A \Delta t}(u^*_{2post} - u^*_{2pre}) \tag{18}$$

$$\sigma_j = \frac{m}{\Delta A \Delta t}(u^*_{1post} - u^*_{1pre}) \tag{19}$$

Heat transfer q follows a similar formulation to temperature.

$$q_j = \frac{m}{2\Delta A \Delta t}(< u_1'^2_{post} > + < u_2'^2_{post} > + < u_3'^2_{post} > - (< u_1'^2_{pre} > + < u_2'^2_{pre} > + < u_3'^2 >_{pre})) \tag{20}$$

References

[1] Bird, G. A., "Molecular Gas Dynamics and the Direct Simulation of Gas Flows," , 1994.

[2] Boyd, I. D., and Schwartzentruber, T. E., *Nonequilibrium Gas Dynamics and Molecular Simulation*, Cambridge Aerospace Series, Cambridge University Press, 2017. https://doi.org/10.1017/9781139683494.

[3] Davis, D. H., "Monte Carlo Calculation of Molecular Flow Rates through a Cylindrical Elbow and Pipes of Other Shapes," *Journal of Applied Physics*, Vol. 31, No. 7, 1960, pp. 1169–1176. https://doi.org/10.1063/1.1735797, URL https://doi.org/10.1063/1.1735797.